JOURNAL OF MATERIALS SCIENCE 19 (1984) 2962–2968

Characterization of microcracks in $YCrO_3$ using small-angle neutron scattering and elasticity measurements

E. D. CASE
Materials and Molecular Research Division, Lawrence Berkeley Laboratory, and Department of Materials Science and Mineral Engineering, University of of California, Berkeley, California 94720, USA

C. J. GLINKA
Reactor Division, National Bureau of Standards, Washington, DC 20234, USA

The mean crack radius, crack opening displacement, number density, and volume fraction have been estimated for a population of microcracks in polycrystalline $YCrO_3$ using small-angle neutron scattering in tandem with elasticity measurements.

1. Introduction

Microcracks are often studied through their effects on various bulk physical properties, including elastic moduli [1–4], thermal diffusivity [5–7], and thermal expansion [8–9]. Direct study of the size, shape and number density of microcracks by surface sensitive techniques, such as the scanning electron microscope (SEM), is difficult because:

1. the stress state at a specimen's surface is not the same as the stress state in the bulk, so the size and number of microcracks that appear on the surface may not be a representative sampling of the bulk microcrack population, and

2. specimen preparation techniques almost invariably damage the specimen surface.

In contrast, small-angle neutron scattering (SANS) yields information for bulk materials about the size, shape and volume fraction of structural inhomogeneities on a scale from about 1 nm to fractions of a micron [10]. Such information is generally derived by comparing the measured angular distribution of the scattered neutrons with calculated scattering curves based on some appropriate physical model for the scattering centres.

In this study, an analysis of SANS data yields estimates for the mean crack opening displacement and volume fraction of microcracks in polycrystalline $YCrO_3$. In addition, the SANS analysis is used in tandem with elasticity measurements to estimate the microcrack number density and the mean crack radius.

$YCrO_3$, which is an orthorhombic perovskite at room temperature, microcracks due to an apparent phase transition at $\sim 1100^\circ$ C. Elasticity measurements indicate microcrack healing for an anneal temperature, T_A, below 1100° C. Subsequent anneals with $T_A > 1100^\circ$ C cause healed specimens to return to their initial, microcracked state. Thus a given $YCrO_3$ specimen can be put into either the healed or microcracked state depending on whether $T_A > 1100^\circ$ C or $< 1100^\circ$ C. Since the $YCrO_3$ specimens are initially sintered at $\sim 1750^\circ$ C, the porosity and grain size are essentially unchanged by the anneals [11], making it possible to vary the microcrack number density without altering other microstructural features. The microstructural invariance is extremely important to SANS work, allowing one to "subtract out" scattering due to porosity and thus independently analyse the neutron scattering due to the population of microcracks.

2. Experimental procedure

The $YCrO_3$ specimens used in this study were prepared from intimately mixed powder precursors of chromium and yttrium. Details of the powder mixing and calcining procedures are given elsewhere [12]. Specimens were isostatically

0022–2461/84 $03.00 + .12

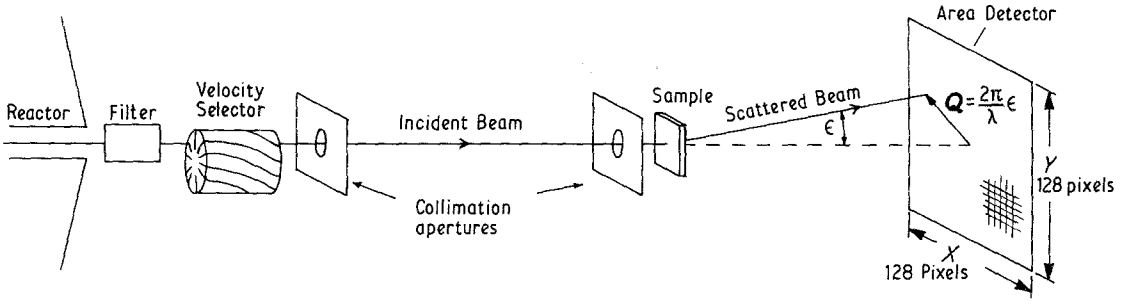

Figure 1 A schematic diagram of the apparatus used for the small-angle scattering measurements. Details of the instrument are given by Glinka [20].

pressed and sintered at 1750° C in flowing forming gas (a 95% nitrogen and 5% hydrogen mixture) in an electric furnace. The resulting $YCrO_3$ billets were cut into prismatic bars using a low speed diamond saw and surface ground to a tolerance of ± 0.005 cm.

The average grain size was ~ 6.0 μm, as determined from the linear intercept technique on scanning electron micrographs of fracture surfaces [13, 14].* Specimen densities, which range from about 92% to 96% theoretical, were calculated from the dimensions and mass of each specimen. X-ray diffraction analysis confirmed that the specimens were in the expected orthorhombic (distorted perovskite) structure at room temperature.

The sonic resonance technique was used for elasticity measurements [15]. All measurements were done at room temperature in air. The experimental technique is discussed in detail by Spinner and Tefft [16]. Elastic moduli were calculated from the resonance frequency data theory developed by Pickett [17] and later modified [18]. Manning [19] reviews the particular computational techniques used.

Small-angle scattering measurements on $YCrO_3$ were carried out at the National Bureau of Standards research reactor [20]. Fig. 1 shows a schematic layout of the SANS instrument. Mean wavelengths, $\bar{\lambda}$, from 0.51 to 0.80 nm (and bandwidth $\Delta\lambda(\text{FWHM})/\lambda = 0.25$) were used in the course of the measurements. Most of the data were taken with $\bar{\lambda} = 0.625$ nm. The scattered neutrons were counted with a 65 cm x 65 cm position-sensitive proportional counter located 3.5 m from the sample in a shielded vacuum chamber. The samples were also maintained under vacuum to minimize background due to air scattering. Specimen transmittances were obtained from the relative intensities of the direct beam, with and without the specimen in place, having first attenuated the beam with a thin cadmium foil (~ 0.1 mm) to eliminate the need to correct the count rates for detector deadtime.

In all cases the observed scattering patterns were circularly symmetric about the beam centre indicating no preferred orientation for the scatterers. The data for each specimen were, therefore, averaged over annular rings, after being corrected for background and specimen transmission, to obtain the net scattering from the sample as a function of the magnitude of the scattering vector, **Q**, where **Q** is defined as

$$\mathbf{Q} = \mathbf{K}_i - \mathbf{K}_f$$

$$|\mathbf{Q}| = \frac{4\pi}{\lambda}\sin(\theta/2) \qquad (1)$$

where θ is the angle between the incident and scattered neutron wave vectors $\mathbf{K}_i$ and $\mathbf{K}_f$ ($K = 2\pi/\lambda$).

In order to estimate the surface area and number of scattering centres, the scattered intensity was calibrated using the incoherent scattering from a water-filled fused silica cell having a flat plate geometry and a 0.2 cm thickness of water normal to the neutron beam. Uncertainties in the multiple scattering corrections make the estimate of the flux from the water scattering accurate to only about ± 30%.

3. Theoretical considerations

Relatively few ceramic materials have been examined with SANS, and in addition, no materials having microcracks or crack-like voids have been studied using SANS. As a first step in the SANS analysis it was necessary to establish whether the

*Grain size measurements were performed for at least one specimen taken from each $YCrO_3$ billet.

neutron scattering was predominantly refractive or diffractive in nature. Information about the size and number of scattering centres can be obtained from either refractive (see, e.g. [23]) or diffractive [10] scattering, but the required analysis is quite different in the two cases.

Theoretical [21, 22] and experimental [22] studies of neutron refraction show that the profile of the transmitted beam depends both on the incident wavelength (λ) and on the thickness of the sample. On the other hand, the shape of scattering due to diffraction phenomena is a function only of the scattering vector, $\mathbf{Q}$, defined in Equation 1.

Because of their quite different functional dependencies, refraction can be distinguished from diffraction experimentally by comparing data taken with different incident wavelengths or with samples of various thicknesses. For the $YCrO_3$ specimens included in this study, the shapes of the experimental scattering curves, when plotted as a function of Q, remain invariant with respect to changes in both the incident wavelength and the specimen thickness, indicating the scattering is predominantly due to diffraction.

For small-angle diffraction, the measured scattered intensity is proportional to a cross-section, $d\Sigma/d\Omega$, which can be expressed quite generally as

$$\frac{d\Sigma}{d\Omega}(\mathbf{Q}) = \frac{1}{V}\left|\int_V \rho(r)\, e^{i\mathbf{Q}\cdot\mathbf{r}}\, dr\right|^2 \qquad (2)$$

where the integration is over the entire specimen volume, V, illuminated by the neutron beam. Thus what is directly measured is the square of a Fourier transform of a scattering density, $\rho(\mathbf{r})$, which contains structural information for the specimen. The density $\rho(\mathbf{r})$ is given by $\bar{b}n$, where $\bar{b}$ is a coherent scattering amplitude [24], averaged over atomic dimensions, and $n(\mathbf{r})$ is the number of nuclei per unit volume at $\mathbf{r}$. For a material consisting of distinct particles* of scattering density ρ_p, imbedded in a matrix of scattering density ρ_m, Equation 2 becomes

$$\frac{d\Sigma}{d\Omega}(\mathbf{Q}) = \frac{1}{V}(\Delta\rho)^2\left|\sum_K \int_{V_{pK}} e^{i\mathbf{Q}\cdot\mathbf{r}}\, dr\right|^2 \qquad (3)$$

where the integration includes the total particle volume and $\Delta\rho = \rho_m - \rho_p$.† If the particles are assumed to be nearly identical, but randomly dispersed throughout the host material, Equation 3 reduces to

$$\frac{d\Sigma}{d\Omega}(\mathbf{Q}) = \frac{V_p^2 N_p}{V}(\Delta\rho)^2 |F_p(\mathbf{Q})|^2 \qquad (4)$$

where $F_p(\mathbf{Q})$ is the single-particle form factor

$$F_p(\mathbf{Q}) = \frac{1}{V}\int_{V_p} e^{i\mathbf{Q}\cdot\mathbf{r}}\, dr \qquad (5)$$

and N_p is the total number of particles, each having volume V_p.

Explicit expressions for $d\Sigma/d\Omega$ are obtained by evaluating Equation 5 for various particle geometries and/or Q ranges. For example, for randomly oriented, sharp-edged scatterers of any given geometry, Guinier [24] has shown that the small Q approximation to Equation 4 is

$$\frac{d\Sigma}{d\Omega} \simeq \frac{N_p(\Delta\rho)^2}{V} V_p^2 \exp(-R_g^2 Q^2/3) \qquad (6)$$

where R_g is the particle's radius of gyration with respect to its centre of gravity.

Similarly, for large Q, Porod [25] has shown that Equation 4 reduces to

$$\frac{d\Sigma}{d\Omega} \simeq \frac{2\pi(\Delta\rho)^2}{V}\frac{S}{Q^4} \qquad (7)$$

where S is the total surface area of the scattering centres contained in the volume, V, illuminated by the neutron beam.

For the special case of randomly oriented thin discs of thickness $2H$ and diameter $2a$, Porod [25] has calculated that Equation 4 reduces to

$$\frac{d\Sigma}{d\Omega}(Q) = \frac{V_p^2 N_p(\Delta\rho)^2}{V}\left(\frac{2}{Q^2a^2}\right)\exp(-Q^2H^2/3) \qquad (8)$$

when $QH < 1 \ll Qa$. The randomly oriented thin disc model should be particularly applicable to scattering from microcracks.

Another approach to describing the scattering from a two-phased material has been developed by Debye *et al.* [26], with the specific problem of a porous material in mind. The model of Debye *et al.* proceeds from the same basic premise that there are only two scattering densities in the problem, a constant ρ_M in the material, and zero when voids represent the second phase. Beyond this, the only further assumption is that the voids be com-

*"Particles" here could refer to precipitates, voids or second phases which are assumed to be sufficiently dilute so that interparticle interference effects can be neglected.

†Note that $\Delta\rho$ refers to a difference in the scattering densities between the matrix and "particle" phases.

pletely random in size, shape, and distribution throughout the material. The observable cross-section for the Debye model is given by

$$\frac{d\Sigma}{d\Omega}(Q) = \frac{8\pi a^3(\Delta\rho)^2\phi(1-\phi)}{(1+Q^2a^2)^2} \quad (9)$$

where the parameter a represents a correlation length, or characteristic void size in the case of a porous solid, and ϕ is the pore volume fraction.

4. Results and discussion

In order to compare the measured neutron scattering curves with the Guinier, randomly oriented thin disc, and Debye models (Equations 6, 8, and 9, respectively) SANS measurements were made on both the microcracked and healed states of a given $YCrO_3$ specimen. After correcting all data for background and specimen transmittance, the neutron scattering contribution from the microcrack population only was calculated from

$$I_{DIFF}(Q) = I_{micro}(Q) - I_{HEALED}(Q) \quad (10)$$

where I_{micro} and I_{HEALED} represent the measured scattered intensity, at a given Q, for the specimen in the microcracked and healed states, respectively. The difference spectra, I_{DIFF}, can then be analysed in terms of the models discussed above.

In Fig. 2 the net scattering, I_{DIFF}, from a 7 mm thick specimen of $YCrO_3$ is plotted on a logarithmic scale against the scattering vector Q. The solid curve in the figure is a porod law, Equation 7, fit to the data which adequately describes the shape of the scattering at larger Q ($Q > 0.003\,nm^{-1}$) but lies systematically below the low Q data. Thus a different functional form is required to represent the data in the small Q region.

Table I gives the results of fitting the I_{DIFF} data for low Q ($0.001\,nm^{-1} \leqslant Q \leqslant 0.0022\,nm^{-1}$) to Equations 6, 8 and 9. The fitting error is estimated by the residual R, defined as

$$R = \frac{\Sigma |I_{DIFF} - I_{fit}|}{\Sigma I_{DIFF}}$$

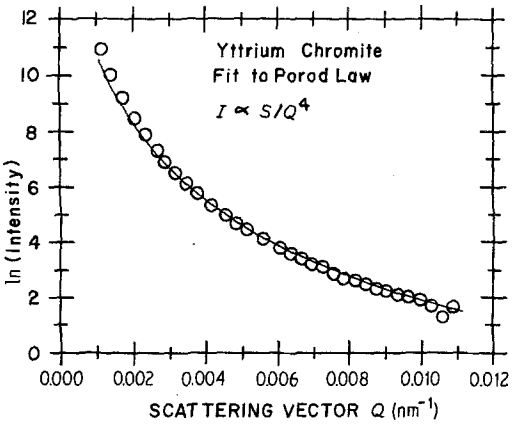

Figure 2 Net scattering (○) due to microcracks from a 7 mm thick specimen of $YCrO_3$ plotted on a logarithmic scale against the scattering vector Q. The curve is a least-squares fit of a Porod law, Equation 7, to the data. The fit is satisfactory at larger Q ($Q \simeq 0.003\,nm^{-1}$) but lies systematically below the data at small Q.

where I_{DIFF} is as defined in Equation 10 and I_{fit} is the fitted intensity value. The randomly oriented thin disc model (Equation 8) yields the smallest residual, indicating, in turn, that the parameter H (which represents half the disc thickness) may be an approximate measure of half the mean crack opening displacement (COD). The fit obtained with the thin disc model is shown in Fig. 3.

Using the high Q data ($0.003\,nm^{-1} \leqslant Q \leqslant 0.011\,nm^{-1}$)* and Equation 7, the total surface area of the microcracks, S, was estimated as $\simeq (1.5 \pm 0.5) \times 10^3\,cm^2$. Thus

$$S = N_c\langle S_c\rangle$$

where N_c is the total number of microcracks and $\langle S_c\rangle$ is the average surface area of a single microcrack. For the thin disc model, where $\langle a\rangle$ is much greater than H,

$$S_c \simeq 2\pi\langle a^2\rangle$$

The number density, n, of microcracks is thus given by

$$n = \frac{S/S_c}{V} = \frac{S}{V}\frac{1}{2\pi\langle a^2\rangle} \quad (11)$$

TABLE I

Model	Functional form	Fitted parameters	R
Randomly oriented thin discs	Equation 7	$H = 12.2 \pm 0.3$ nm	0.022
Guinier	Equation 6	$R_g = 17.5 \pm 0.5$ nm	0.070
Debye	Equation 9	$A = 50 \pm 40$ nm	0.045

*The high Q data include 52 points, all of which were normalized to the scattering from water.

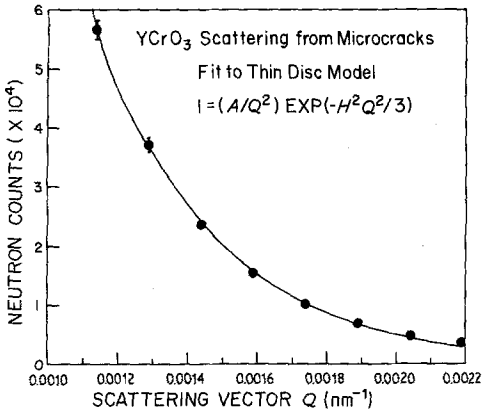

Figure 3 The data points are the low Q scattering from microcracks in a 7 mm thick specimen of $YCrO_3$. The curve is a least-squares fit to the data of the scattering function for randomly oriented thin discs of thickness $2H$.

Rearranging Equation 11 and using the measured value of S yields

$$n\langle a^2\rangle = \frac{S}{2\pi V} \simeq 3.4 \times 10^2\,\mathrm{cm}^{-1} \qquad (12)$$

An estimate for $\langle a\rangle$, the mean crack radius, may be obtained by using Equation 12 in conjunction with elasticity data. For randomly oriented microcracks, Budiansky and O'Connell [28] relate the microcrack-induced decrement in the bulk Young's modulus, Y, and Poisson's ration, ν, to a crack density parameter, ϵ, where

$$\epsilon = n\langle a^3\rangle \qquad (13)$$

and

$$Y = Y_0\left[1 - \frac{16(1-\nu^2)(10-3\nu)\epsilon}{45(2-\nu)}\right] \qquad (14)$$

In Equation 14, Y_0 and ν_0 refer to the Young's modulus and Poisson's ratio of the unmicrocracked body, respectively, while Y and ν refer to the microcracked state.

From elasticity measurements, $Y_0 \simeq 220$ GPa, $Y \simeq 90$ to 110 GPa, $\nu_0 = 0.28$, and $\nu = 0.14$, which (using Equation 14) yields the estimate $\epsilon \simeq 0.29$.

An estimate for $\langle a\rangle$ can be obtained from

$$\epsilon/n\langle a^2\rangle = \frac{\langle a^3\rangle}{\langle a^2\rangle} \simeq 1.5\langle a\rangle, \qquad (15)$$

where the evaluation of $\langle a^3\rangle/\langle a^2\rangle$ is discussed in the Appendix. Using Equations 12 and 15, the mean crack radius, $\langle a\rangle$, is approximated by $\langle a\rangle \simeq 5.7\,\mu$m. This $\langle a\rangle$ estimate corresponds well with the measured average grain size of 6 μm, which is in agreement with the model of localized stress inducing microcracks that are approximately one to several grain diameters in length [6, 29, 30]. For a COD of $2H$ (~ 25 nm), this gives a crack aspect ratio of ~ 1.5 to 3.5×10^{-3}, which again is in rough agreement with observed microcrack aspect ratios observe for several materials [6, 31].

The volume fraction of microcracks can be determined from the SANS measurement as

$$\frac{\Delta V}{V} = \frac{N_c(\pi a)^2(2H)}{V} = \frac{SH}{V} \qquad (16)$$

where, in this case, V, the volume illuminated by the neutron beam is 0.7 cm^3. Using $H = 12.2$ nm and $S = 1.5 \times 10^3\,\mathrm{cm}^3$ yields

$$\frac{\Delta V}{V} \simeq 2.6 \times 10^{-3}.$$

Batzle *et al.* [32] and O'Connell and Budiansky [33] have found, for geological materials, volume fractions of microcracks ranging from $\sim 1 \times 10^{-3}$ to 5×10^{-3}. Using Equation 12, and noting that $\langle a^2\rangle/\langle a\rangle^2 = 4/\pi$ (Appendix) the crack number density may be estimated as

$$n \simeq 8.2 \times 10^8\,\mathrm{cm}^{-3}.$$

5. Conclusions

The mean crack radius, crack opening displacement, number density, and volume fraction have been estimated for a population of microcracks in polycrystalline $YCrO_3$. To the authors' knowledge, this study represents the first analysis of these microcrack parameters in a bulk ceramic, although there have been SANS studies of pores in ceramics. This procedure could be applied to other materials, if microcracked and nonmicrocracked specimens of a given material have similar populations of background scatterers (such as pores, inclusions, etc.) allowing such scattering contributions to be subtracted off and the remaining scattering to be analysed in terms of models, such as the thin disc, that are appropriate for scattering from microcracks.

The crack opening displacement, $2H$, and the volume fraction of cracks, $\Delta V/V$, can be obtained directly from the SANS data, using the low Q, thin disc approximation for $\Delta V/V$. The mean crack radius, $\langle a\rangle$, and the crack number density, n, can be obtained by combining the SANS analysis with a complementary elasticity analysis. It should be

emphasized that the elasticity analysis yields only the product $n\langle a^3\rangle$, and the Porod approximation gives the product $n\langle a^2\rangle$. However, one can use the elasticity and SANS data in tandem to estimate $\langle a\rangle$ and n.

Acknowledgements

The authors acknowledge the help of T. Negas, Inorganic Materials Division, National Bureau of Standards, Washington, D.C., and L. P. Dominques, Trans-Tech, Inc., Gaithersburg, Maryland, in the preparation of high purity sintered polycrystalline $YCrO_3$ billets, from which the authors prepared specimens for elasticity and SANS analysis. This work was supported in part by the Lawrence Berkeley Laboratory. In addition, one of the (E. D. Case) gratefully acknowledges support from a National Research Council postdoctoral associateship during part of this work.

Appendix

Grain size distributions in a polycrystalline material have often been described in terms of Rayleigh or lognormal distributions [34, 36]. The general form of the Rayleigh probability distribution, $p_r(x)$ is given by

$$p_r(x) = bx \exp(-cx^2) \quad \text{for } x \geqslant 0$$

The normalization condition

$$\int_0^\infty bx \exp(-cx^2)\, dx = 1$$

requires that $b = 2c$. If x is distributed according to the Rayleigh distribution, then $\langle x\rangle$, the mean of x, is given by

$$\langle x\rangle = 2\int_0^\infty bx^2 \exp(-bx^2)\, dx = \left(\frac{\pi}{4b}\right)^{1/2}$$

The second moment, $\langle x^2\rangle$, and the third moment, $\langle x^3\rangle$, are given by

$$\langle x^2\rangle = 2\int_0^\infty bx^3 \exp(-bx^2)\, dx = \frac{1}{b}$$

$$\langle x^3\rangle = 2\int_0^\infty bx^4 \exp(-bx^2)\, dx = 3/2\left(\frac{1}{b}\right)\left(\frac{\pi}{4b}\right)^{1/2}$$

Thus,

$$\langle x^3\rangle/\langle x^2\rangle = \left(\frac{\pi}{4b}\right)^{1/2}(3/2) = 1.5\langle x\rangle$$

Therefore, if the grain radius, a, in $YCrO_3$ is distributed according to the Rayleigh distribution, this would give

$$\langle a^3\rangle/\langle a^2\rangle = 1.5\langle a\rangle \qquad \text{(A1)}$$

The lognormal probability distribution function, $p_l(D)$, can be expressed as [34, 37],

$$p_l(D) = \frac{1}{(2\pi\sigma^2)^{1/2}}\frac{1}{D}\exp[-(\ln D - \mu)^2/2\sigma^2]$$

where σ = the standard deviation of $\ln D$ and μ = the value of $\ln D$ averaged over the pdf. The jth moment of the lognormal distribution is given by [34]

$$\langle D^j\rangle = D_{\text{med}}^j \exp(j^2\sigma^2/2)$$

where D_{med} refers to the median value of D. Thus,

$$\frac{\langle D^3\rangle}{\langle D^2\rangle} = D_{\text{med}} \exp(5\sigma^2/2) = \langle D\rangle \exp(2\sigma^2) \qquad \text{(A2)}$$

If D is the equivalent spherical diameter of a grain, then $\sigma \approx \frac{1}{2}$, by both experimental observation and theoretical considerations [34, 35]. For $\sigma \approx \frac{1}{2}$, Equation A2 gives

$$\frac{\langle D^3\rangle}{\langle D^2\rangle} \simeq 1.6\langle D\rangle$$

or, equivalently in terms of a, the grain radii,

$$\frac{\langle a^3\rangle}{\langle a^2\rangle} = 1.6\langle a\rangle \qquad \text{(A3)}$$

Therefore, whether the grain size distribution is Rayleigh or lognormal, Equations A1 and A3 give approximately the same results for the ratio of the third moment to the second moment.

References

1. R. R. SUCHOMEL and O. HUNTER, JR, *J. Amer. Ceram. Soc.* **59** (1976) 149.
2. E. D. CASE, J. R. SMYTH and O. HUNTER, JR, *J. Nucl. Mater.* **102** (1981) 135.
3. *Idem, Mater. Sci. Eng.* **51** (1981) 175.
4. J. A. KUSZYK and R. C. BRADT, *J. Amer. Ceram. Soc.* **56** (1973) 420.
5. H. J. SIEBENECK, D. P. H. HASSELMAN, J. J. CLEVELAND and R. C. BRADT, *ibid.* **60** (1977) 336.
6. W. J. BUYKX, *ibid.* **62** (1979) 326.
7. N. CLAUSSEN and J. JÜRGEN, *Ber. Dtsch. Keram. Ges.* **55** (1978) 487.
8. W. R. MANNING, O. HUNTER, JR, F. W. CALDERWOOD and D. W. STACY, *J. Amer. Ceram. Soc.* **55** (1972) 342.
9. O. D. SLAGLE, *Carbon* **7** (1969) 337.
10. G. KOSTORZ, in "Treatise on Materials Science and Technology", Vol. 15, edited by G. Kostorz (Academic Press, New York, 1979) pp. 227–89.
11. E. D. CASE, T. NEGAS and L. P. DOMINGUES, unpublished data (1982).

12. T. NEGAS and L. P. DOMINGUES, in "Fourth International Meeting on Modern Ceramics", edited by P. Vincenzini (Elsevier Interscience, New York, 1979) p. 993.
13. R. L. FULLMAN, *Trans. AIME* **1973** (1953) 447.
14. E. D. CASE, J. R. SMYTH and V. LOCKE, *Commun J. Amer. Ceram. Soc.* **64** (1981) c-24.
15. F. FORSTER, *Z. Metallk.* **29** (1937) 109.
16. S. SPINNER and W. E. TEFFT, *ASTM Proc.* **61** (1961) 1221.
17. G. PICKET, *ibid.* **45** (1945) 846.
18. D. P. H. HASSELMAN, "Tables for the computation of shear modulus and Young's modulus of rectangular prisms" (Carborundum Co, Niagara Falls, NY, 1961).
19. W. R. MANNING, PhD thesis, Iowa State University, Ames, IA (1970).
20. C. J. GLINKA, "AIP Conference Proceedings No. 89, Neutron Scattering – 1981", edited by J. Faber, p. 395.
21. R. VON NARDROFF, *Phys. Rev.* **28** (1926) 240.
22. R. J. WEISS, *ibid.* **83** (1951) 379.
23. P. PIZZI, "Symposium on Fracture Mechanics of Ceramics", Vol. 3, edited by R. C. Bradt, D. P. H. Hasselman, and F. F. Lange, (Plenum Press, New York, 1973).
24. A. GUINIER, "X-Ray Diffraction" (Freeman, San Francisco, 1963) Ch. 10.
25. G. POROD, *Acta Phys. Austriaca* **2** (1948) 255.
26. P. DEBYE, H. R. ANDERSON and H. BRUMBERGER, *J. Appl. Phys.* **28** (1957) 679.
27. J. WALSH, *J. Geophys. Res.* **74** (1969) 4333.
28. B. BUDIANSKY and R. J. O'CONNELL, *Int. J. Solids Struct.* **12** (1975) 81.
29. R. W. DAVIDGE and G. TAPPIN, *J. Mater. Sci.* **3** (1968) 297.
30. H. P. KIRCHNER, *J. Amer. Ceram. Soc.* **53** (1970) 232.
31. W. F. BRACE, E. SILVER, K. HADLEY and C. GOETZE, *Science* **18** (1972) 162.
32. M. L. BATZLE, G. SMIMMONS and R. W. SIEGFRIED, *J. Geophys. Res.* **85** (1980) 7072.
33. R. J. O'CONNELL and B. BUDIANSKY, *ibid.* **79** (1974) 5412.
34. S. K. KURTZ and F. M. A. CARPAY, *J. Appl. Phys.* **51** (1980) 5725.
35. *Idem, ibid.* **15** (1980) 5745.
36. N. LOUAT and J. E. MORALL, *Met. Trans.* **5** (1974) 2616.
37. J. AITCHINSON and J. A. C. BROWN, "The Lognormal Distribution" (Cambridge University Press, Mass., 1957).

Received 18 November
and accepted 24 November 1983